Characterization of Local Plasma Parameters during High Power ICRH discharges at TEXTOR*

K. Crombé[1, 2], C. C. Klepper[3, §], E. A. Unterberg[3], O. Schmitz[4], J. Ongena[1], J. W. Coenen[4], T. K. Gray[3], A. Pospieszczyk[4], M. Vervier[1], T. Wauters[1] and TEXTOR team

[1]Association EURATOM-Belgian State, Royal Military Academy, Brussels, Belgium; [2]Department of Applied Physics, Ghent University, Belgium; [3] Oak Ridge National Laboratory, Oak Ridge, TN 37831-6169, USA; [4] Assoc. EURATOM-FZJ, Trilateral Euregio Cluster, 52425 Jülich, Germany.
[§]Corresponding Author

Introduction

Local electron density (n_e) and temperature (T_e) profiles are critical inputs for Ion Cyclotron-resonance Heating (ICRH) antenna modeling and already shown to have the greatest impact on coupling through the plasma boundary [1]. Furthermore, the local interaction between the antenna and the boundary plasma can locally alter the conditions of the boundary plasma. In fact, recent work in ICRH antenna modeling predicts significant, local n_e depletion [2]. Experimental verification of this effect would be valuable for antenna model validation. Another area that would benefit from direct measurement would be the detection of DC electric fields expected to form by rectification of the parallel to the confining toroidal magnetic field components of the injected RF electric fields [3]. Such DC electric fields are expected to be substantial (few kV/cm) and form on plasma-facing components, such as protective limiters or protective tiles of antenna plena, which might intercept magnetic field lines passing in front of the face of the antenna. Although measurement of near-antenna RF electric fields by Stark-effect spectroscopy was recently demonstrated [4], the measurement of the DC sheath fields has proven to be more difficult, partly owing to their much smaller spatial extent.

The experiments described herein are a continuation of ICRH antenna physics studies related to EFDA Task No. *WP12-IPH-A11-3-06/PS-01*, originally written to emphasize the ITER-relevant need for neutral density n_{neut} profiles in front of an ICRH antenna, but has since expanded to include n_e, T_e profiles (needed to interpret hydrogen/deuterium H_α/D_α measurements) as well as efforts to measure local electric fields via Stark-effect spectroscopy.

In this paper we describe a first set of n_e, T_e profiles, measured at one of the TEXTOR antennas with high-power (>~1MW/antenna) ICRH injection, then compared with similar neutral beam injection (NBI) heated discharges. We also provide first observation of Stark-effect spectroscopy-relevant spectra. Initial D_α data for n_{neut} profile determination were also collected, but are outside the scope of this paper.

The availability of dedicated, high-power ICRH operation on TEXTOR, combined with TEXTOR's unsurpassed flexibility of optical access provided the opportunity for these parallel efforts.

Experimental Setup.

A detailed description of the (super-) thermal He beam-enhanced spectroscopic arrangement, called *HELIOS*, can be found in Ref [5]. The system now features:

- Highly collimated (~1°) and moduled (>~10ms), low fluence (<10^{18} neutrals) thermal helium (He) beam probing the top region of the ICRH antenna (Fig. 1). It is recalled that antenna modeling predicts strongest local sheath effects at top/bottom ends of antennas (e.g. Ref. [6])

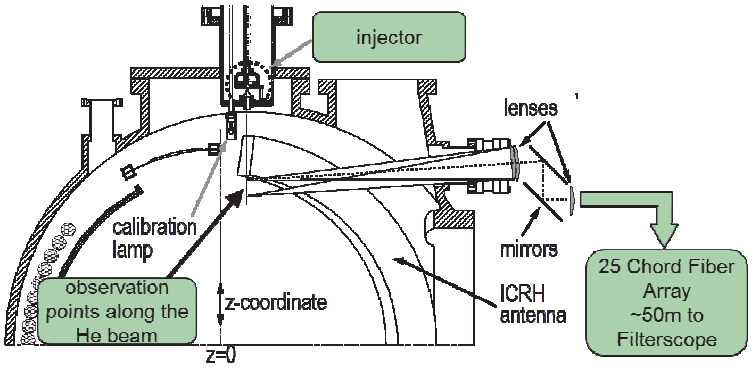

Figure 1. Illustration of spectroscopic set-up to measure n_e, T_e (,N_{neut}) locally at the ICRH antenna.

- A 25-fiber optical collection array, providing 2mm resolution, as well as flexibility in plasma positioning.
- Each optical view is simultaneously sampled by four filtered detectors, providing time-resolved intensities for three He I lines used to determine n_e, T_e and D_α used for n_{neut}.

Independently of the HELIOS diagnostic, a high-resolution, optical spectrometer was deployed to sample a region of the *Gen-2* ICRH antenna plenum, where a broad-beam, thermal He neutral injector was embedded to enhance local He I emission.

Measured Trends in the Antenna-local Plasma Parameters

Experiments carried out in L-mode discharges using both TEXTOR ICRH antennas, denoted as *Gen-1* and *Gen-2*. For some of the shots, one NBI line (*NBI-2*) was used to keep total power constant, as ICRH power varied. The other line (*NBI-1*) was kept on for all discharges. The profiles were measured at *Gen-1*, while the high resolution spectroscopy was at *Gen-2*.

A large database of He I (for n_e, T_e) and D_α intensities were collected in the campaign. Figure 2 shows time traces for a typical shot sequence in the campaign. This constitutes the first use of this matured, multi-chordal, high spatial and spectral resolution diagnostic for a wide range of plasma conditions and ICRH antenna power levels.

The measurement points in the bottom row of graphs of Fig. 2 are not processed n_e and T_e values, but rather raw ratios of He I intensities, one mainly sensitive to n_e and one to T_e. The data is sampled at 100 kHz but is down-sampled, through ensemble averaging, to 1 kHz. The grey bands in these graphs denote when the HELIOS He injection is active (~120 ms every 500 ms). Even at this stage of the analysis, one begins to see a significant drop in the density-sensitive ratio, when the RF is on. There is a corresponding rise in the temperature-sensitive ratio, but it appears to be much smaller. (The region of interest is highlighted with schetch-in circle on top of the data points in the figure).

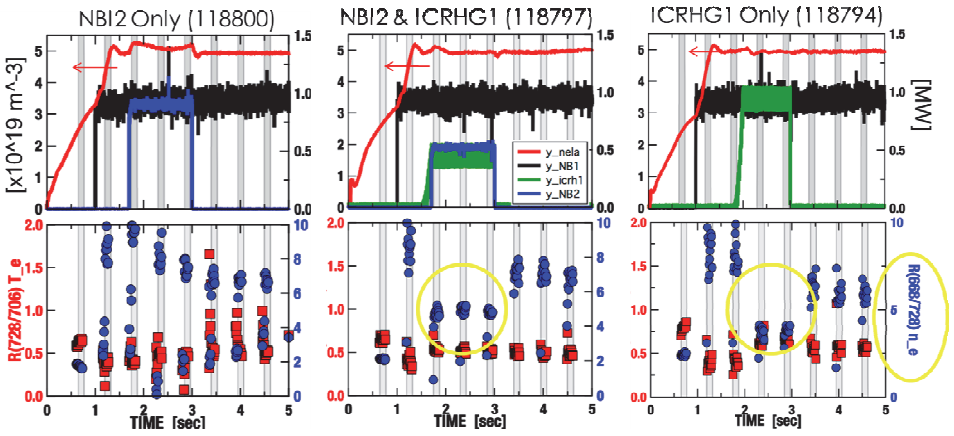

Figure 2. Top Row: Time traces of line-averaged core plasma density, NBI and ICRH (Gen-1 and Gen-2 antenna powers). Bottom Row: Unprocessed (i.e. CRM not yet applied) line ratios representative of n_e and T_e at the antenna Gen-1. Main thing to note here is that local n_e clearly drops when the observed antenna is on. This was one of the higher powers reached with this (Gen-1) antenna; the Gen-2 antenna reached a 1.5MW/ant level during this experimental campaign.

Processed Plasma Parameter Profiles

The plasma parameters are computed from the line ratios by applying factors produced by collisional-radiative modelling (CRM) and tabulated into look-up tables. Two CRMs are in use in this study. One is static and the other dynamic, in that it takes into account the dynamics of long lifetime, metastable states contributing to the CR of the He I lines of interest [7]. In Fig. 3, processed n_e and T_e profiles with and without RF (but at constant power through the separatrix) are shown for a 1MW case.

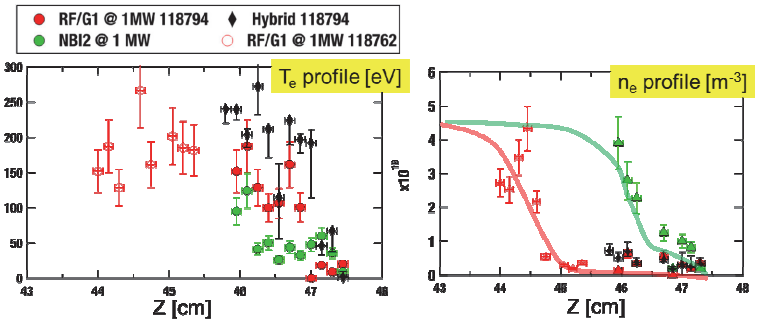

Figure 3. Comparison of ICRH-only and NBI-only shots at the same total power. The ICRH profile is over a longer vertical extent by combining data from 2 similar shots, with the 2nd shot using a second set of the fiber array. (There were less "filterscope" channels than there were optical fibers and corresponding views). The solid lines are sketched-in and only suggestions of the likely trend suggested by the data.

The most notable feature is a clear drop in n_e near the antenna with ICRH. Whether the apparently corresponding rise in T_e is significant needs further study. The points labeled *Hybrid* correspond to the same, RF-on raw data, but analysed with the dynamic CRM model (also referred to as *hybrid model*). In general, the hybrid model tends to yield much higher Te values for the same ratios for the conditions of interest in the antenna boundary-layer plasma. The discrepancy in n_e values is much smaller [7]. Preliminary analysis indicates that the drop in the local n_e scales roughly with local antenna RF power.

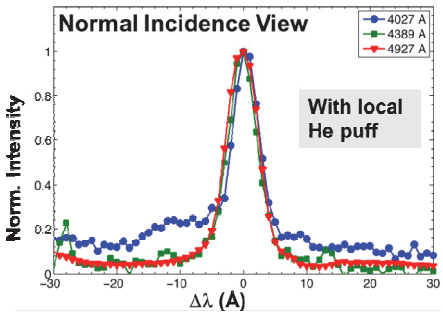

Figure 4. Candidate He I lines: 4027 Å, 4389 Å and 4927 Å for the detection of strong electric fields via Stark-mixing (satellites)

He I Spectra

All three, candidate, high n-state, **He I** lines [8] were clearly detectable (Fig. 4) -
4388Å [2^1P-5^1D], 4027Å[2^1P-5^1D], 4927Å [2^1P-5^1D].
In an earlier campaign, without the local He puff, only one (4388Å) was detected but with S/N ~ 2.

However, satellites were not detected, possibly obscured by background (from unperturbed neutrals). Interfering feature on tails of the 4027Å line further complicated the analysis.

Discussion, Conclusions and Upcoming Work

Results indicate a correlation between localized n_e drop and RF power at the location of measurement under similar total input power. This is consistent with present modeling results predicting n_e depletion due the ponderomotive forces developed by interaction of the near-field waves with the strong magnetic field (B_t) present in front of the antenna [2]. Detection of this effect constitutes an important step toward validation of ICRH antenna models, which are in turn used to design antennas for next generation fusion devices.

Toward the end of the experimental campaign, TEXTOR was operated with reverse B_t (normally B_t is anti-parallel to I_P) and some preliminary effects on the profiles were detected. However the antennas required more conditioning to get to the same high powers. A follow-up campaign is being proposed to revisit this study with reversed-B_t. Sweeping q_{edge} to vary magnetic connections is also envisioned.

Regarding the Stark-mixing He I satellites study, the measurements indicated that local He puffing greatly enhances signal of the (generally weak) high n-states spectral lines needed for this study. However, the predicted satellites were not detected. It is possible that the local He puff increased the unperturbed background (emission from region outside the sheath). A tangential spectrometer view, "grazing" the plenum surface with 2mm resolution, to maximize collection from the sheath, was also deployed but not equipped with high dynamic range detector. Plans for the proposed follow-up campaign include measurement with grazing view using a high dynamic range detector.

*** This work was supported, in part, by EURATOM and carried out within the framework of the European Fusion Development Agreement. The views and opinions expressed herein do not necessarily reflect those of the European Commission. This work was also supported by the US DOE under Contract No. DE-AC05-00OR22725 with UT-Battelle, LLC**

References

[1] A. Messiaen and R. Weynants, 2011 *Plasma Phys. Control. Fusion* **53** 085020
[2] Dirk Van Eester, Kristel Crombé and Volodymyr Kyrytsya, 2013 *Plasma Phys. Control. Fusion* **55** 025002
[3] O.A. D'Ippolito, J.R. Myra, M. Bures et al., *Plasma Physics and Controlled Fusion* **33**, No.6, 607 (1991)
[4] C.C. Klepper et al., 2013 *Phys. Rev Lett.* **110**, Issue 21, id. 215005.
[5] E.A. Unterberg, et al., 2012 *Rev Sci Instrum*. **83** (10): 10D722. doi: 10.1063/1.4739236.
[6] L. Colas et al., *Nucl. Fusion* **45** (2005) 767–782
[7] J.M. Muñoz-Burgos et al. *PoP* (2012) 012501
[8] B.M. Obradović, M.M. Kuraika, *Phys Lett A* **372** (2008) 137-140